10-1-2003

Structural Analysis of Gelsolin Using Synchrotron Protein Footprinting

Janna G. Kiselar
Case Western Reserve University, janna.kiselar@case.edu

Mark R. Chance
Case Western Reserve University, mark.chance@case.edu

Author(s) ORCID Identifier:

Mark R. Chance

Recommended Citation

Janna G. Kiselar, Paul A. Janmey, Steven C. Almo, Mark R. Chance. Structural Analysis of Gelsolin Using Synchrotron Protein Footprinting. Molecular & Cellular Proteomics, Volume 2, Issue 10, 2003, Pages 1120-1132, https://doi.org/10.1074/mcp.M300068-MCP200.

Structural Analysis of Gelsolin Using Synchrotron Protein Footprinting*

Janna G. Kiselar‡§, Paul A. Janmey¶, Steven C. Almo§‖, and Mark R. Chance‡§‖**

Protein footprinting provides detailed structural information on protein structure in solution by directly identifying accessible and hydroxyl radical-reactive side chain residues. Radiolytic generation of hydroxyl radicals using millisecond pulses of a synchrotron "white" beam results in the formation of stable side chain oxidation products, which can be digested with proteases for mass spectrometry (MS) analysis. Liquid chromatography-coupled MS and tandem MS methods allow for the quantitation of the ratio of modified and unmodified peptides and identify the specific side chain probes that are oxidized, respectively. The ability to monitor the changes in accessibility of multiple side chain probes by monitoring increases or decreases in their oxidation rates as a function of ligand binding provides an efficient and powerful tool for analyzing protein structure and dynamics. In this study, we probe the detailed structural features of gelsolin in its "inactive" and Ca^{2+}-activated state. Oxidation rate data for 81 peptides derived from the trypsin digestion of gelsolin are presented; 60 of these peptides were observed not to be oxidized, and 21 had detectable oxidation rates. We also report the Ca^{2+}-dependent changes in oxidation for all 81 peptides. Fifty-nine remained unoxidized, five increased their oxidation rate, and two experienced protections. Tandem mass spectrometry was used to identify the specific side chain probes responsible for the Ca^{2+}-insensitive and Ca^{2+}-dependent responses. These data are consistent with crystallographic data for the inactive form of gelsolin in terms of the surface accessibility of reactive residues within the protein. The results demonstrate that radiolytic protein footprinting can provide detailed structural information on the conformational dynamics of ligand-induced structural changes, and the data provide a detailed model for gelsolin activation. ***Molecular & Cellular Proteomics 2:1120–1132, 2003.***

Hydroxyl radicals, generated through the radiolysis of water using synchrotron radiation, can efficiently oxidize aromatic and sulfur-containing amino acids on the surface of proteins in direct relation to their reactivity and their solvent accessibility (1, 2). In particular, the solvent-accessible side chains of cysteine, methionine, phenylalanine, tyrosine, tryptophan, histidine, proline, and leucine provide convenient probes for synchrotron footprinting experiments (3). These residues cover around 30% of the sequence of a typical protein and thus provide multiple probes that offer significant coverage of the entire macromolecule (prowl.rockefeller.edu/). The radiolytic footprinting approach is illustrated in Fig. 1. Following digestion of irradiated protein solutions with proteases, the products are separated by reverse-phase liquid chromatography and analyzed by electrospray ionization mass spectrometry. The amounts of modified and unmodified peptides are individually quantitated for a specific exposure time, and the rate of oxidation of peptides containing the susceptible sites is determined by measurements at varying exposure times (1, 2, 4–6). This approach is very similar to deuterium exchange mass spectrometry (MS)[1] methods (7–11), except that the side chains instead of the backbone positions are probed and that the covalent nature of the modifications permits the application of a wide variety of proteases, chromatographic separations, and tandem MS approaches to identify the site of modification.

Three features of radiolytic footprinting as detailed here assure that the intact population of molecules is probed. First, the rate of loss of the unmodified fraction is examined, emphasizing the disappearance of biologically intact material. Second, the total dose is limited, and third, the observation of a first-order process in the loss of the unmodified fraction assures that no dose-dependent change in reactivity is induced by the oxidations. These safeguards are the hallmark of all footprinting approaches, which depend on the covalent modification or cleavage of macromolecules to probe the structure (12, 13). The rates of oxidation are analyzed in the context of available structural data, from which the solvent accessibility of the side chains of interest can be calculated. The power of the method is most apparent in examining the changes in structure upon ligand binding, as the oxidation rates of a particular peptide site may increase, decrease, or stay the same in response to ligation. Each of these possible results is informative in terms of protein structure, dynamics, and mechanism.

Gelsolin is an actin-binding protein that has been implicated in remodeling the actin cytoskeleton during numerous cellular processes. It can sever actin filaments as well as bind and cap

From the Departments of ‡Physiology and Biophysics and ‖Biochemistry and the §Center for Synchrotron Biosciences, Albert Einstein College of Medicine, Bronx, New York, 10461-1602 and the ¶Institute for Medicine and Engineering, University of Pennsylvania, Philadelphia, Pennsylvania 19104

Received, July 10, 2003, and in revised form, September 8, 2003
Published, MCP Papers in Press, September 8, 2003, DOI 10.1074/mcp.M300068-MCP200

[1] The abbreviations used are: MS, mass spectrometry; MS/MS, tandem mass spectrometry; ESI, electrospray ionization.

the fast growing barbed end (14, 15). Gelsolin is activated by Ca^{2+} and inhibited by polyphosphoinositides (14–17). The protein, composed of six homologous subdomains (termed S1–S6), exists in a cytoplasmic form and plasma form and is known to have nanomolar and micromolar affinity Ca^{2+} binding sites (18). All six subdomains have a similar folding topology consisting of a central five- or six-stranded β-sheet sandwiched between a long α-helix running approximately parallel to the strands and a shorter α-helix running approximately perpendicular to the strands (17). The crystallographic structure of the inactive Ca^{2+}-free form of equine plasma gelsolin has a compact globular shape; the S1–3 and S4–6 halves of the molecule are connected by a long linker forming extensive interactions between the S6 domain and S1–S3. Specifically, individual β-sheets of S1 and S3 form an extended β-sheet, while S2 and S3 are connected by an extended 30-residue stretch that runs over the central sheet of S1. An extended β-sheet is also formed between S4 and S6; a long loop of 22 amino acids connects S5 and S6. Thus, the organization of S1 relative to S3 and the organization of S4 relative to S6 are similar. However, the positioning of S2 relative to S1 and S3 is different compared with S5 in relation to S4 and S6.

The N-terminal half of the molecule is implicated in severing actin filaments, whereas the C-terminal half of gelsolin appears to function as a regulatory domain that senses the intracellular Ca^{2+} concentration and signals this event to the N-terminal half (19). In particular, the helical C-terminal helix of S6 (termed the "latch") directly contacts the F-actin binding helix of S2 (17) making its actin binding sites inaccessible in the absence of Ca^{2+}. Upon Ca^{2+} activation gelsolin undergoes substantial changes in structure, involving a number of rearrangements that reveal actin filament and actin monomer binding sites (20–23). Thus, the side chains associated with these rearrangements are predicted to have different rates of oxidation in the absence and presence of Ca^{2+}.

Recently, we examined Ca^{2+}-dependent oxidation for a number of peptides within gelsolin. We showed that five of the analyzed peptides experience Ca^{2+}-dependent increases in oxidation rate, while two peptides exhibit Ca^{2+}-dependent protections. Quantitative Ca^{2+} titration isotherms described a three-state equilibrium activation of gelsolin, and specific structures for the activated intermediates were proposed (4). In this paper we provide a more complete analysis, including measurement of the oxidation rate of 81 (of 85 possible) tryptic peptides in gelsolin, and evaluate the oxidation rates (or lack of oxidation) on the basis of side chain surface accessibilities derived from the Ca^{2+}-free gelsolin structure. The Ca^{2+}-dependent changes in oxidation of these peptides are also examined to understand the activated state, for which explicit structural data have been previously unavailable. Tandem MS of each oxidized peptide identifies the specific side chain probes that report structural alterations. We identify 38 side chains throughout the molecule that are sufficiently surface-accessible to permit oxidation; the variation in the oxidation of these probes specifically locates the sites sensible to the Ca^{2+}-dependent conformational change. In addition, the probes that are not oxidized (but intrinsically reactive) also specify sites in the molecule that do not become significantly exposed in the activation process. The results demonstrate the specific residues buried in the inactive gelsolin structure that become more accessible in the calcium activation process. These include residues in the C-terminal helical tail that contact the F-actin binding helix as well as residues indicated as participating in the F-actin binding site. Finally, we use the data to illustrate the potential applications of the footprinting method to a wide range of questions involving protein structure and dynamics.

EXPERIMENTAL PROCEDURES

Sample Preparations and Experimental Design—Recombinant human plasma gelsolin was prepared by the method of Wen *et al.* (24). Prior to radiolysis experiments, protein was dialyzed against 10 mM cacodylic acid sodium salt trihydrate, 0.5 mM EGTA (≥99.0%, Fluka Chemical Corporation, Milwaukee, WI) buffer, pH 7.0, at 4 °C with three changes. The extinction coefficient at 280 nm of 1.4 ml/(mg·cm) (25) was used to determine the gelsolin concentration. For the dose-response experiments, the protein concentration was adjusted to 10 μM. Samples for the EGTA-treated form of gelsolin (calcium-free form of the protein) were used as described above. The Ca^{2+} concentration was calculated to be <1 nM using computer program WEBMAXC, version 2.10 (Stanford University, 2000) (26). For the Ca^{2+}- activated form, $CaCl_2$ (99.99%, Aldrich) was added to the protein, which contained 10 mM cacodylic acid sodium salt trihydrate and 0.5 mM EGTA, to achieve a calculated free Ca^{2+} concentration of 0.2 mM. The buffer and $CaCl_2$ solutions were prepared using nanopore-filtered water and stored in plastic vessels. Less than 120 nM contaminating free Ca^{2+} was measured in 10 mM cacodylic acid sodium salt trihydrate buffer, pH 7.0, using the fluorescent Ca^{2+} indicator Fura-2 (Molecular Probes, Inc., Eugene, OR). The free Ca^{2+} concentrations for the buffers containing EGTA and/or Ca^{2+} were calculated using the computer program WEBMAXC, version 2.10 (Stanford University, 2000) (26), which includes a number of parameters including buffer conditions, nucleotide, temperature, and ionic strength. A 5-μl portion of each protein solution was dispensed into a 0.7-ml microcentrifuge tube for radiolysis and stored on ice for ~3 h prior to use. Radiolysis experiments were performed at ambient temperature.

Synchrotron X-ray Radiolysis—Radiolysis experiments were performed at beamline X28C of the National Synchrotron Light Source of the Brookhaven National Laboratory (Long Island, NY) (1, 27, 28). An electronic shutter equipped with a platinum/iridium alloy aperture (Vincent Associates, Rochester, NY) was used to control the millisecond exposure times. All experiments were performed at a ring energy of 2.8 giga electron volts and at a beam current between 183 and 195 mA (1, 4). The sample tubes with 5 μl of protein solution were positioned in a holder and held parallel to the x-ray beam. The beam dimensions were adjusted to irradiate the entire sample using computer-based alignment. After exiting the beamline, the photons exit the storage ring beam pipe through a beryllium window and travel within the hutch through air over 50 cm before reacting with the sample. Two sets of samples were exposed to x-ray for 0, 20, 40, 80, and 160 ms.

Proteolysis—Irradiated proteins in 10 mM cacodylic acid sodium salt trihydrate, 0.5 mM EGTA buffer, pH 7.0, were digested at 37 °C with 1:50 w/w sequencing grade modified trypsin (Promega Corporation, Madison, WI) for 12 h. Digestion was terminated by freezing the samples.

Mass Spectrometric Analysis—The extent of oxidation in the radio-

lytic peptides was determined using a Finnigan (San Jose, CA) LCQ quadrupole ion trap mass spectrometer equipped with an electrospray ion source. Digested protein solutions were directed into the ion source with a flow rate of 50 μl/min using an Alliance 2690 Waters Corporation (Milford, MA) high pressure liquid chromatography system via a VYDAC (Hesperia, CA) 1.0 × 150-mm reverse-phase C_{18} column. Proteolytic peptides were eluted from the column with a gradient of acetonitrile of 1%/min. Mass spectra were recorded in the centroid mode. ESI-MS/MS spectra were acquired to identify sites of amino acid side chain oxidation (30, 31) and interpreted manually with the aid of the ProteinProspector (University of California, San Francisco, CA) and PAWS (Proteometrics, New York, NY) algorithms.

Modification Rates Calculation—The fraction unmodified was calculated from the ratio of the area under the ion signals for the unoxidized peptides to the sum of those for the unoxidized peptides and their radiolytic products (totals). Background modification seen for the methionine-containing peptides in the unexposed sample was subtracted from the totals. The fraction unmodified for each individual peptide at each time point was normalized to the fraction at zero exposure time, where the fraction unmodified is 1.0 (one). The fraction-unmodified peptide was fit to the equation $Y = Y_0\, e^{-kt}$ using the Origin 6.0 (Microcal Software, Inc., Northampton, MA) program, where Y and Y_0 are the fraction of unmodified peptide at a time t and 0 (seconds), respectively, and k is a first-order rate constant. Dose-response curves are presented as the unmodified fraction (plotted on a logarithmic scale) *versus* x-ray exposure time.

Side Chain Solvent Accessibility Calculation—The VADAR computer program (PENCE, University of Alberta, Edmonton, Alberta, Canada) was used to calculate the solvent-accessible surface areas of all side chains (Å^2). The crystal structure of calcium-free equine plasma gelsolin (Protein Data Bank code 1D0N) was selected for this analysis. Human plasma gelsolin shares 95% of its sequence with equine plasma gelsolin.

RESULTS AND DISCUSSION

Footprinting Strategy to Examine the Structure of Calcium-free Gelsolin—Ca^{2+}-free gelsolin was exposed to the x-ray beam for intervals ranging from 0 to 160 ms and then digested with trypsin as described under "Experimental Procedures." Because synchrotron radiolysis induces covalent changes in the protein structure, it is important to ensure that the oxidations do not influence the data derived from the technique. The levels of oxidation are controlled by using the minimum exposure time necessary to generate detectable signals. With millisecond time scale exposures, oxidative modifications dominate the chemistry compared with cleavage events and cross-linking (2, 29). Moreover, because surface residues are primarily oxidized, resulting in polar substitutions of side chains, the effects on the global protein structure are typically minimal. Thus, the irradiation dose is optimized to produce oxidations of reactive sites with minimal perturbation of the protein and to generate data that is first-order for the loss of unmodified material.

Following digestion of the protein with trypsin, the peptide products were quantitatively analyzed by mass spectrometry coupled to high performance liquid chromatography as described under "Experimental Procedures." Examining the loss of unmodified fraction for particular peptides provides a rate constant that is sensitive entirely to the unmodified population. In contrast, analyzing the rate of formation of the modified population would directly measure the oxidation of already oxidized material. Moreover, the dose-response curves derived from data analysis are extrapolated to zero fraction modified, reflecting the first-order process indicative of constant reactivity consistent with a low dose regime. If the structure was altered by modification (for example resulting in protein unfolding), the oxidation rate as a function of dose would likely increase, and the dose-response curve would be nonlinear. Because the reaction rates correlate with measures of solvent accessibility of the residue side chains within the protein structure, comparison of the oxidation rates of various peptides for the Ca^{2+}-free and Ca^{2+}-activated gelsolin provides structural comparisons relevant to the activation process.

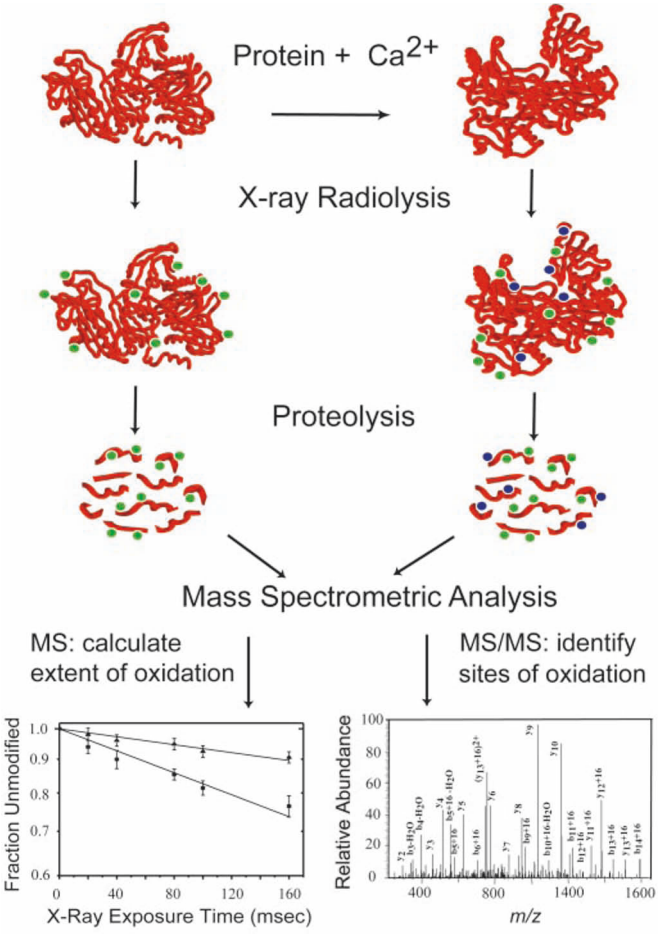

FIG. 1. **A schematic representation of synchrotron radiolysis and mass spectrometry experiments.** Proteins in the absence and presence of Ca^{2+} are exposed to the synchrotron x-ray beam. *Green* schematically indicates the oxidation sites in the absence and presence of Ca^{2+}. *Blue* indicates the sites that were oxidized only in the presence of Ca^{2+}. Oxidized proteins are subjected to proteolysis and MS, which is employed to quantitatively measure the extent of modification. The specific oxidation site(s) are determined by MS/MS. Dose-response profiles are plotted for each modified peptide. Modification rates for proteolytic peptides derived from Ca^{2+}-free and Ca^{2+}-activated gelsolin forms are calculated and compared.

Identification of Oxidized Peptide Products from Ca^{2+}-free

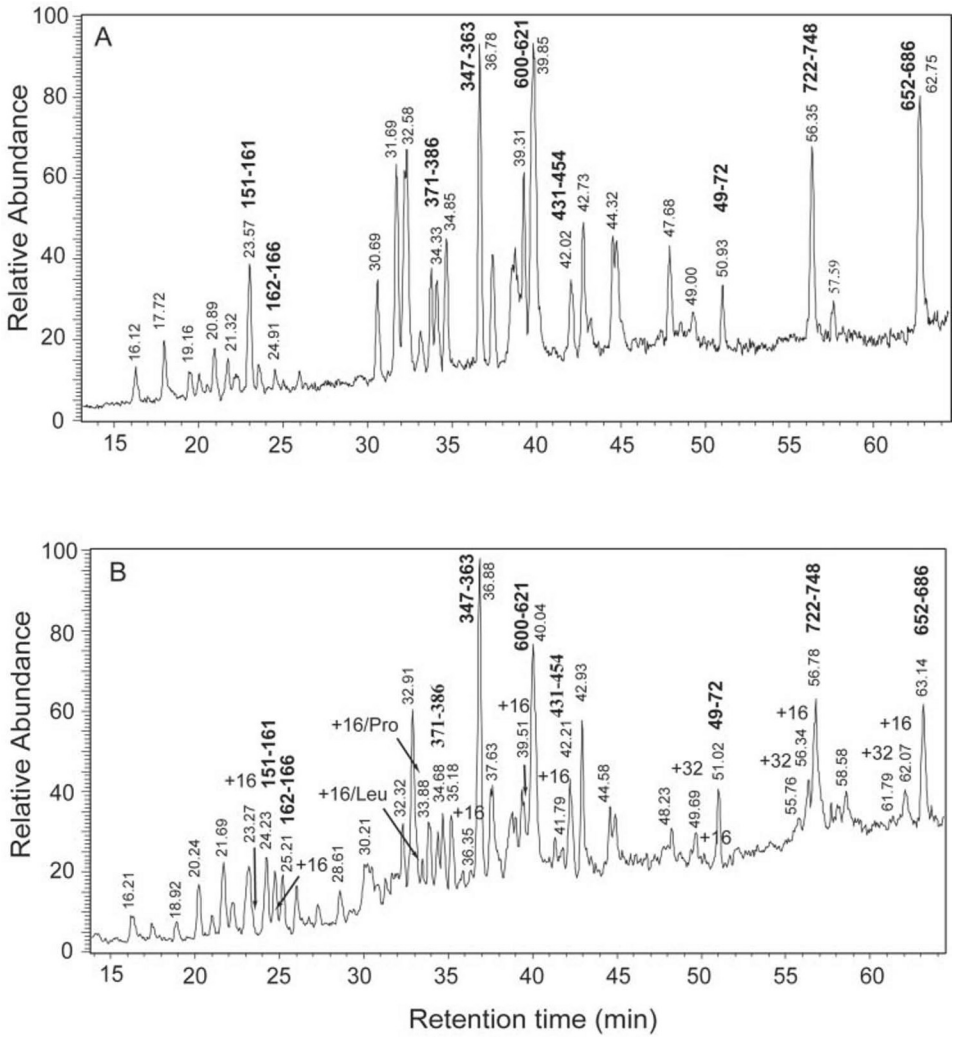

FIG. 2. **The representative total ion current chromatograms for the tryptic digest of gelsolin exposed for (*A*) 0 and (*B*) 80 ms, respectively.** Additional peaks corresponding to the oxidation products are marked *+16* or *+32*.

Gelsolin—The protease digestion of the oxidized protein sample results in the formation of peptides and their stable oxidation products that are readily separated by the gradient of the reverse-phase chromatography and quantitated using ESI mass spectrometry. The total ion current chromatograms of the tryptic digest of gelsolin before (*panel A*) and after (*panel B*) radiolysis for 80 ms are shown in Fig. 2. Nine peptides are labeled in this chromatogram for illustration. The chromatogram in *panel B* clearly indicates additional peptide peaks (marked *+16* or *+32*) that correspond to the oxidized peptides that appear after protein exposure. Because the proteolytic peptides and their oxidized products have in most cases very similar structure and a molecular mass that is shifted by +16 or +32 atomic mass units (corresponding to the addition of one or two oxygens, respectively), the ionization and detection efficiencies of these peptides are relatively comparable. However, because the oxygen adducts result in the formation of more polar peptides, the retention time is typically reduced. For example, the modified product for peptide segment 722–748 (Fig. 2*B*) that incorporated one oxygen was eluted from the column a half-minute prior to its unoxidized parent peptide, whereas the same peptide modified by two oxygens was detected about 1 min prior to the unoxidized peptide. However, in the case of protein segments with an oxidized methionine residue, the retention time for peptides with one or two incorporated oxygens can be several minutes less than the unoxidized peptide. For example, a methionine-containing peptide comprised of residues 652–686 that was modified by one and two oxygens was eluted from the column 2 and 3 min prior to the unmodified peptide, respectively (Fig. 2*B*). By careful examination of the chromatogram, the unoxidized and oxidized products for each peptide can be identified. Of 85 total tryptic peptides expected for gelsolin, 81 peptides were detected in the chromatogram (resulting in 95% coverage of the gelsolin sequence); the identity of these peptides was verified by MS/MS sequencing. Twenty-one

TABLE I

Rate constants for the oxidation of gelsolin peptides at 0 and 200 μM Ca^{2+}

Data for some of the peptides have been reported previously (4).

Domain Segment	Sequence	Oxidized Amino Acid(s)	Rate of Modification at Reactive residues(s) (sec^{-1}) 0mM [Ca^{2+}]	0.2mM [Ca^{2+}]
S1 22-34	PNSMVVEHPEFLK - - 84 10 89	Met25	87.14 ± 3.93	86.38 ± 11.08
S1 38-45	EPGLQIWR 60 26 6	Pro39	0.44 ± 0.09	0.41 ± 0.06
S1 49-72	FDLVPVPTNLYGDFFTGDAYVILK 109 0 60 45 7 37 0 6 0 0	Phe49, Tyr59	1.47 ± 0.09	2.24 ± 0.13
S1 87-115	YWLGNECSQDESGAAAIFTVQLDDYL 9 0 23 10 0 53 13 NGR	Tyr111	1.86 ± 0.13	1.93 ± 0.13
S1 121-135	EVQGFESATFLGYFK 76 0 13 13 11	Phe125	0.69 ± 0.05	0.98 ± 0.10
S2 143-150	GGVASGFK 105	Phe149	0.48 ± 0.03	0.50 ± 0.03
S2 151-161	HVVPNEVVVQR 10 67	Pro154	0.80 ± 0.06	0.78 ± 0.04
S2 162-166	LFQVK 0 0	Phe163	-	0.35 ± 0.05
S2 173-207	ATEVPVSWESFNNGDCFILDLGNNIH 89 11 0 0 1 24 27 QWCGSNSNR 0	Pro177	1.27 ± 0.09	1.18 ± 0.07
S2 231-250	VHVSEEGTEPEAMLQVLGPK 31 31 1 63 2 123	Leu244, Pro249	0.78 ± 0.06	0.76 ± 0.05
S2 251-262	PALPAGTEDTAK 74 3 86	Pro251, Pro254	0.58 ± 0.05	0.58 ± 0.03
S3 276-300	VSNGAGTMSVSLVADENPFAQGALK 3 74 28 3 5	Met283	16.11 ± 1.80	2.07 ± 0.12
S3 342-346	MDYPK 54 22 86	Met342	97.31 ± 18.96	93.97 ± 13.97
S3 347-363	QTQVSVLPEGGETPLFK 0 18 12 67 1	Leu361	0.19 ± 0.02	0.23 ± 0.04
S3-S4 371-386	DPDQTDGLGLSYLSSH 116 97 9 15 6 38	Pro372 Leu378, Tyr382	0.38 ± 0.05 0.30 ± 0.05	0.47 ± 0.06 0.40 ± 0.06
S3-S4 393-420	VPFDAATLHTSTAMAAQHGMDDDGT 108 12 2 96 6 29 3 GQK	Pro394, Met406 Met412	12.86 ± 3.21	9.33 ± 1.12
S4 424-438	RIEGSNKVPVDPATY 89 94 45	Pro432, Pro435 Tyr438	0.78 ± 0.09	0.71 ± 0.09
S4 431-454	VPVDPATYGQFYGGDSYIILYNYR 89 94 45 1 33 1 14 0 5	Pro432, Pro435 Tyr438, Tyr442	1.05 ± 0.10	1.74 ± 0.19
S5 571-588	TPSAAYLWVGTGASEAEK 91 19 3 0	Pro572, Tyr576	0.84 ± 0.09	0.78 ± 0.08
S5 600-621	AQPVQVAEGSEPDGFWEALGGK 19 69 1 19 4	Pro611, Trp615	1.17 ± 0.04	1.15 ± 0.08
S6 652-686	FVIEEVPGELMQEDLATDDVMLLDT 10 13 8 72 0 1 0 0 WDQVFVWVGK 66 5 0	Met662	78.35 ± 40.10	7.22 ± 2.26
S6 722-748	QGFEPPSFVGWFLGWDDDYWSVDPL 101 0 0 1 12 0 104 10 28 16 24 6 DR	Phe724,Leu734, Tyr740	1.91 ± 0.15	3.26 ± 0.20

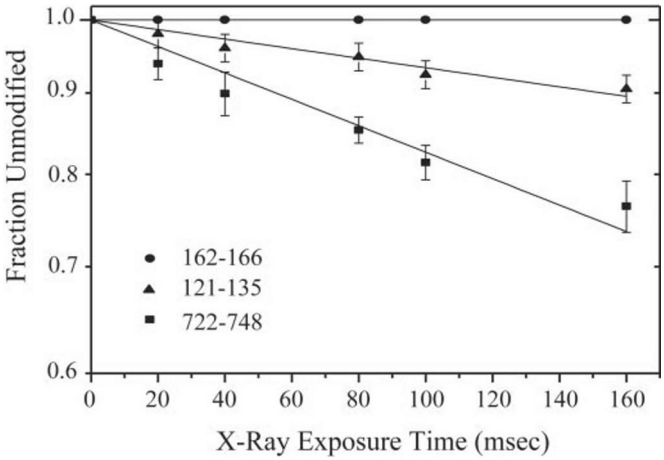

FIG. 3. **The representative dose-response curves for the oxidation of three peptides after radiolysis of Ca^{2+}-free gelsolin.** Peptide 162–166 (S2) showed no oxidation. The peptides comprised of residues 121–135 (S1) and 722–748 (S6) exhibited modifications ranging from modest to highly oxidized, respectively.

peptides were detected to be oxidized for the inactive gelsolin sample, and the extent of the oxidation was measured for each peptide at each synchrotron dose (time of exposure). The fraction of unoxidized peptide was calculated from the ratio of the area under the ion signal for the unmodified peptides to the total peptide (sum of ion signals for the unoxidized peptides and their radiolytic products). Dose-response curves for all oxidized peptides were constructed by plotting the fraction unmodified (on a log scale) for each peptide as a function of exposure time. Duplicate (or triplicate) experiments revealed that variations in the measured fraction of unmodified peptide at any exposure time were less than 1.5% and were not observed to exceed 2.5% in absolute value. First-order rate constants for all oxidized peptides in the absence of Ca^{2+} were derived from this analysis as described previously (1, 2, 4, 6); the rates of oxidation are shown in Table I.

Representative dose-response curves for three of these peptides are shown in Fig. 3. The data are the average of two independent experiments with the *error bars* representing the range of values observed. The quality of the data and the adherence to first-order behavior are apparent. It is also clear that different peptides have significantly different rates of oxidation. These rates range from no detectable oxidation for peptide 162–166 within S2 to a rate of 0.69 $\pm$ 0.05 s^{-1} for peptide 121–135 within S1, while peptide 722–748 within S6 is oxidized at a rate of 1.91 $\pm$ 0.15 s^{-1}. The oxidation rate data for all peptides are shown in Table I; 21 peptides had detectable levels of oxidation in the absence of Ca^{2+}, while 60 peptides did not exhibit oxidation (data of this type are shown only for peptide 162–166 in Table I). These observations suggest that most of the reactive side chain residues are buried inside the structure consistent with the highly compact crystal structure. Also, this is an important result for the method because these buried residues remain unreactive throughout the experiment; they are "canaries in the coal mine." If oxidation is disrupting protein structure, the interior of the protein would be expected to become solvent-exposed. The peptide segment 162–166 (part of the F-actin binding site) in the EGTA conformation of gelsolin represents a typical buried probe of this kind. It contains two modifiable residues (leucine and phenylalanine) that have 0 $Å^2$ solvent accessibility (Table I).

Correlation of Footprinting and Crystallographic Data for Ca^{2+}-free Gelsolin—The following reactivity order for side chain modification of small peptides in an unhindered steric environment (*i.e.* highly accessible) under synchrotron radiolysis has been reported: Cys, Met > Phe, Tyr $\geq$ Trp > Pro > His, Leu (3). This is consistent with pulse radiolysis data where the rate of reaction of hydroxyl radicals with isolated amino acids has been measured (30). However, as demonstrated for gelsolin above, in the case of proteins, oxidations occur only on the reactive residues that are accessible. Knowing the values for the side chain accessible surface areas ($Å^2$) for all amino acids within the gelsolin sequence, we can predict the potentially modifiable residues in the experiment. The theoretical measures of solvent accessibility were calculated as described under "Experimental Procedures" using the available crystal structure of Ca^{2+}-free equine plasma gelsolin (17). Because the human plasma and equine plasma gelsolin share 95% sequence identity, similar accessibilities are expected. The reactive residues within the 21 oxidized peptides of Ca^{2+}-free gelsolin with their side chain accessible surface areas printed immediately below the one-letter code are shown in Table I. We have reported previously a positive correlation between reactivity of a particular side chain residue and its solvent accessibility (1, 2, 5, 6); this correlation is evident in the data here. For example, the peptide composed of residues 121–135 has five potentially reactive amino acids: Phe-125, Phe-130, Leu-131, Tyr-133, and Phe-134 with calculated solvent-accessible side chain surface areas of 76, 0, 13, 13, and 11 $Å^2$, respectively (Table I). Thus, phenylalanine at position 125 is $\sim$5$\times$ more accessible to the solvent than the other four residues and expected to be the most likely candidate for oxidation (this is proven by MS/MS below). Moreover, the reaction rate for peptide 121–135 was calculated to be 0.7 s^{-1}, which is approximately one-half the rate of peptide 49–72 ($\sim$1.5 s^{-1}). Consistent with this rate difference, the first peptide contains a highly reactive residue with a side chain accessible surface area of $\sim$76 $Å^2$, whereas the second peptide has two equally reactive residues with a total side chain accessible surface area of $\sim$150 $Å^2$. On the other hand, peptides comprising residues 301–311, 334–341, 538–542, 694–701, and 715–721 contain potentially reactive amino acid side chains, including Cys-304 (4.7 $Å^2$), Phe-305 (2.8 $Å^2$), Leu-307 (0.3 $Å^2$), Phe-338 (0.4 $Å^2$), Leu-538 (0.1 $Å^2$), Phe-539 (0.0 $Å^2$), Leu-697 (41.0 $Å^2$), and Pro-716 (3.5 $Å^2$), that are not sufficiently accessible to the solvent to provide detectable reactivity under these conditions (data not shown).

Overall, there are 186 potentially reactive residues (based

on the eight typically observed) distributed across the entire protein sequence. Of these 186 amino acids, 60 residues are completely inaccessible (0.0 Å^2) to the solvent and were unreactive in Ca^{2+}-free gelsolin under the radiolysis conditions applied. Thirty-four of the potentially reactive sites exhibited oxidation (Table I). All oxidized residues were compared with the theoretical measures of the solvent accessibility calculated for Ca^{2+}-free gelsolin. As a result of this analysis, the threshold values of detection for phenylalanine and tyrosine side chains were determined to be >14 Å^2 in the solvent-accessible surface area of the side chain group; for tryptophan the threshold value is >18 Å^2, while for proline and leucine side chains, the accessibility had to be above >60 Å^2 for the detection of modification. This reactivity order is similar to what is seen for model peptides, but the exact detection thresholds above are specific for this experiment and depend on exposure times, beam flux, sample concentrations, and buffer conditions.

For methionine the results are more complicated. For example, substantial oxidation was observed for Met-283, -406, and -412 despite the low theoretical measures of solvent accessibility that were calculated. In previous studies we suggested that one of the possible explanations for this phenomenon may lie in a different mechanism of oxidation, including electron transfer from close-by, solvent-accessible residues (1). Thus, the methionine residues not only appear to probe the solvent-accessible surface of the side chain but also are sensitive to the local environment within 5–8 Å. On the other hand, the theoretical measures of the solvent accessibility for Met-243, -509, -517, and -635 were calculated to be 1, 14, 0, and 14 Å^2, respectively, and no oxidation was observed for these residues. Also, for Met-342 and -662 the accessibility is 54 and 72 Å^2, respectively, and a high oxidation rate for the peptides containing these residues was observed. In addition, Met-25 is disordered in the crystallographic structure and was found to be reactive in our experiments. These observations suggest that Met-25 may be solvent-accessible. For six amino acids within the Ca^{2+}-free gelsolin sequence, including Pro-30, Leu-33, Leu-287, Tyr-344, Pro-345, and Trp-677, oxidation was not observed. Because they are located in peptides that contain highly accessible and reactive methionine residues, methionine oxidation dominated for these peptides.

Overall the observed modified residues are distributed throughout the protein; thus, they provided sufficient coverage of the structure such that we can analyze structural changes for each of the six domains of gelsolin independently with several probes each. It is also important to emphasize that overall, the peptide oxidation data are consistent with the crystallographic data for inactive gelsolin, and this demonstrates that our footprinting approach reliably probes the protein structure. Furthermore, because the solvent accessibility on the surface of the protein in various buffer conditions can be monitored by this technique, changes in the solvent accessibility of the specific sites of gelsolin during Ca^{2+} activation can provide valuable information on the structural reorganization of the gelsolin surface.

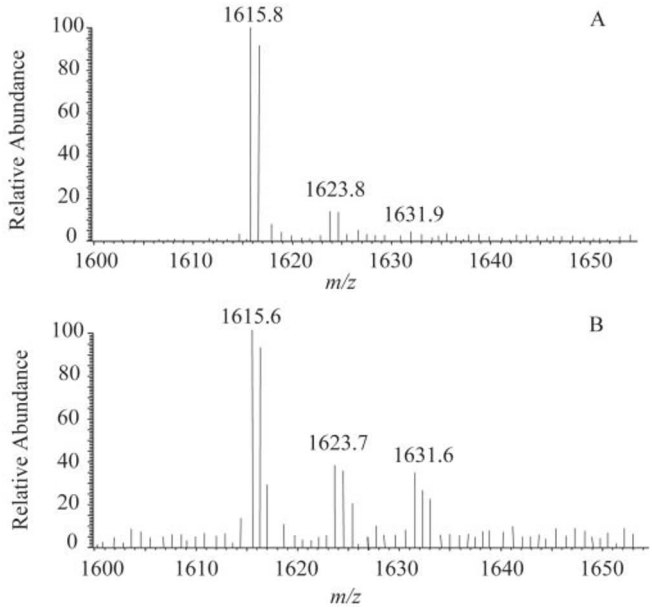

FIG. 4. **The representative electrospray mass spectra for region 722–748 and its radiolytic products after exposure for 80 ms to synchrotron light at Ca^{2+} concentrations of (*A*) <1 nM and (*B*) 200 μM.** The unmodified ion appears at *m/z* 1615.8. The peak ions at *m/z* 1623.8 and 1631.9 represent the radiolytic products corresponding to the addition of one and two oxygens, respectively, on the side chains of phenylalanine, leucine, and tyrosine residues.

Ca^{2+}-dependent Conformational Rearrangements of Gelsolin—Gelsolin containing 200 μM Ca^{2+} was exposed for 0–160 ms and then digested with trypsin in the manner described above. Quantitative mass spectrometric analysis reveals that in the presence of 200 μM Ca^{2+} 22 peptides showed oxidation compared with 21 that were modified for calcium-free gelsolin. Specifically, peptide 162–166 showed oxidation only upon calcium addition. Of 22 modified segments of the protein, seven exhibited changes in their oxidation rates as a function of calcium. A representative electrospray mass spectrum is shown in Fig. 4 for one peptide (residues 722–748) after exposure to 80 ms of synchrotron light at low (*panel A*) and 200 μM (*panel B*) Ca^{2+} concentrations. The unmodified peptide 722–748 is detected as a doubly protonated ion at *m/z* 1615.8. The peaks at *m/z* 1623.8 and 1631.8 represent the radiolytic products corresponding to the addition of one and two oxygens, respectively, on the side chains of phenylalanine, leucine, and tyrosine residues within this peptide. It is clear from mass spectra that at 200 μM Ca^{2+} concentration the relative abundance of the modified peaks is significantly larger contributing to a larger fraction of modified peptide upon calcium addition.

Dose-response curves for all 22 oxidized peptides were obtained from the ESI-MS data of the digested protein and analyzed. Dose-response curves for selected peptides, including the seven that were calcium-sensitive (*panels I–O*) and eight that were not (*panels A–H*), are presented in Fig. 5. The

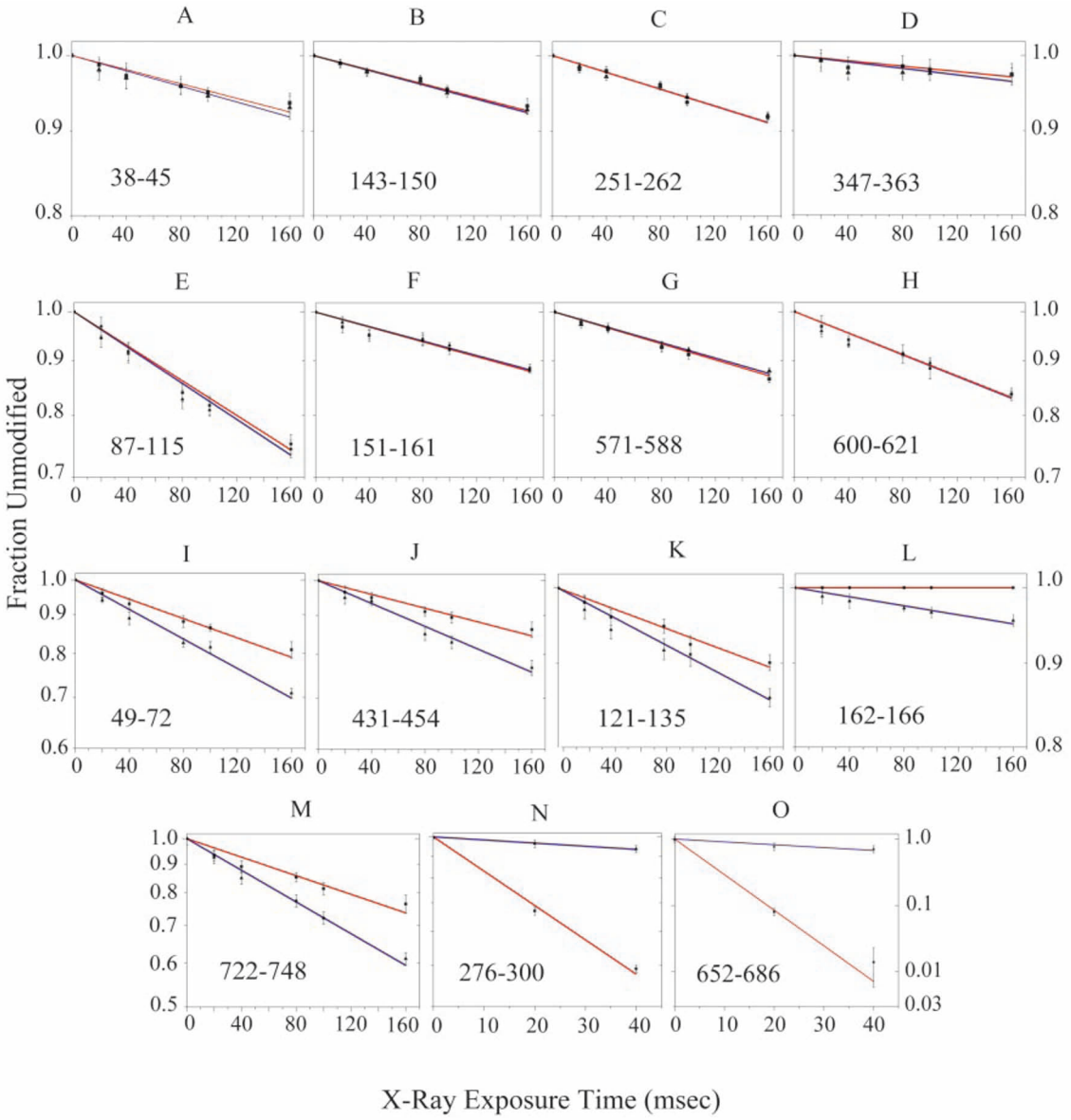

FIG. 5. **Dose-response curves for the oxidation of the gelsolin peptides at Ca^{2+} concentrations of <1 nM (■) and 0.2 mM (▲) as a function of exposure time.** *A–O*, these figures represent data for 15 oxidized peptides. *I–M*, five peptides showed increases in oxidation rate at 200 μM Ca^{2+} including peptides comprised of residues 49–72, 121–135, 162–166, 431–454, and 722–748. *N–O*, dose-response curves for two methionine-containing peptides comprised of residues 276–300 and 652–686 show dramatic decreases in the oxidation rate as the Ca^{2+} concentration was elevated to 200 μM. *A–H*, data for peptides comprised of residues 38–45, 87–115, 143–150, 151–161, 251–262, 347–363, 571–588, and 600–621 showed no changes in oxidation rate in the presence of 200 μM Ca^{2+}.

values plotted in this figure are the average of two independent experiments, and the *error bars* represent the range of values observed. Among the peptides that changed their oxidation rate as a function of calcium, peptides 49–72 and 121–135 within S1 had 40–50% increases in their modification rates at 200 μM Ca^{2+} compared with the case for calcium-free gelsolin. Peptide 162–166 (part of the F-actin binding site on S2) exhibited an increase in the rate of oxidation upon Ca^{2+} binding consistent with an increased exposure of Phe-163. Unfortunately, the other F-actin binding site on S2, including residues 209–230, could not be analyzed because of the absence of any modifiable amino acid. For the peptide comprised of residues 431–454 (S4 β-sheet), the extent of modification was calculated to be 65% higher upon gelsolin activation. The largest increase in the oxidation rate (70%) was observed for peptide 722–748, which is consistent with the location of the peptide within S6 and the helical tail of the protein. Two segments comprised of amino acids 276–300 and 652–686 exhibited dramatic decreases in reactivity. For example, peptide 276–300 (S3) showed an 87% decrease in

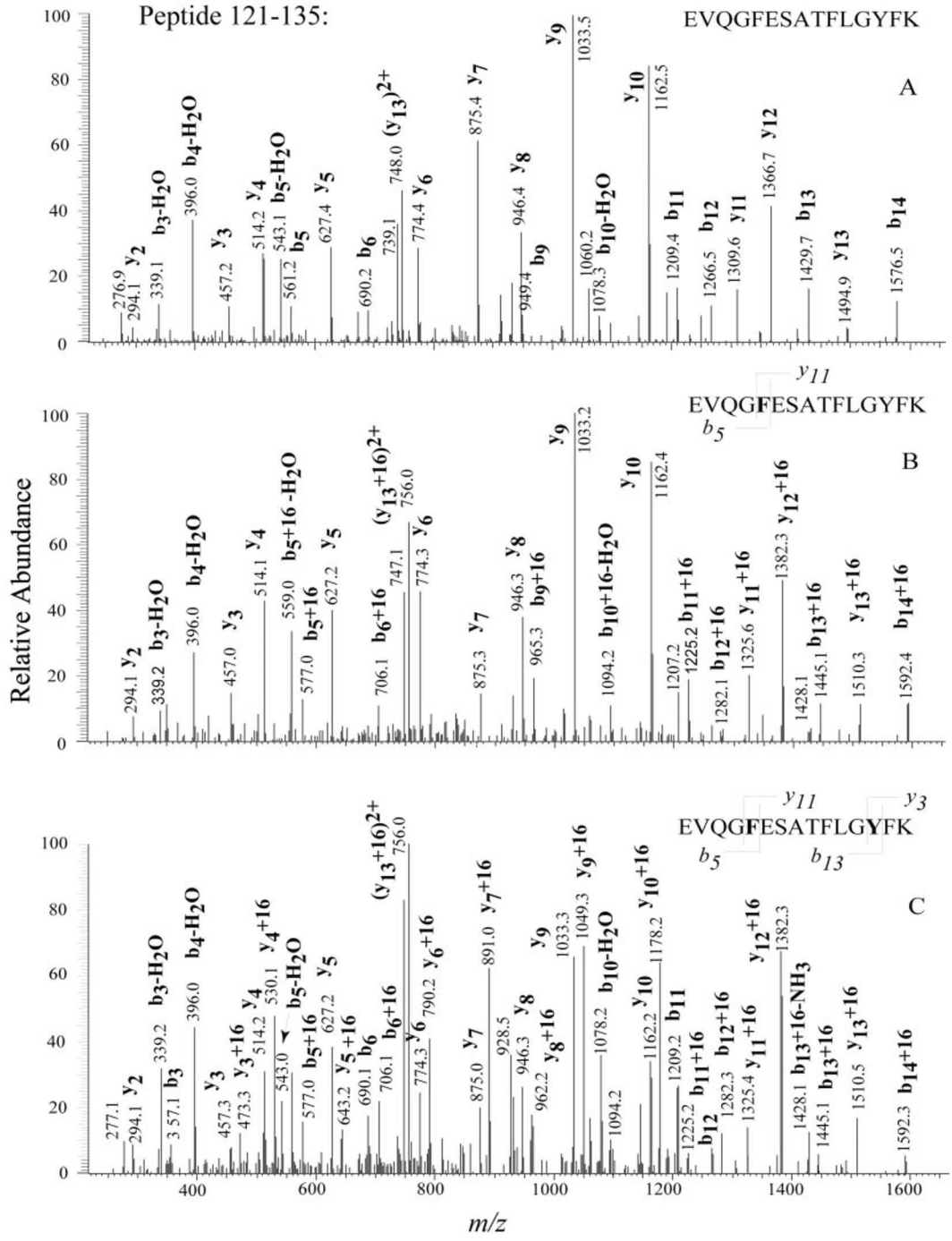

FIG. 6. **MS/MS spectra of the peptide comprised of residues 121–135.** *A*, MS/MS spectrum of the unoxidized peptide. *B*, MS/MS spectrum of the oxidized radiolytic product of the same peptide from the exposure of protein solution (containing <1 nM Ca^{2+}) to the x-ray beam for 80 ms. *C*, MS/MS spectrum of the oxidized products of the same peptide from the exposure of the protein solution (containing 200 μM Ca^{2+}) to the x-ray beam for 80 ms.

the rate of oxidation, whereas peptide 652–686 (S6) showed a decrease of 90% (4). Because these protein regions contain highly reactive methionine residues, substantial oxidation occurred at very short exposure times; thus, the dose-response data was truncated at 40 ms to restrict the quantitation to the region where the data is first-order. Also, the error in the rate determination appears to be significantly higher than the other peptides (1). Nevertheless, protections as a function of Ca^{2+} are clearly observed (Fig. 5, *panels N* and *O*).

Identification of Oxidation Sites by Tandem Mass Spectrometry—Tandem mass spectrometry was performed to determine the specific site or sites of oxidation for each oxidized

peptide and to potentially detect any changes in the specific site of oxidation as a function of the ligand. Fig. 6 shows representative ESI-MS/MS spectra upon selection of the doubly charged ion (*m/z* 862.0) of peptide 121–135 (*panel A*) and its singly oxidized radiolytic product (+*16*) in the absence of calcium (*panel B*) and the +16 modified product in the presence of calcium (*panel C*). The y_n or b_n fragment ions observed represent cleavage products of the peptide bond with charge retention in the C- or N-terminal end of the peptide, respectively (31, 32). The sequence for the unmodified peptide 121–135 can clearly be read from the spectrum in Fig. 6*A*; this is the control experiment for comparison so as to determine the location of the potentially modified (shifted) daughter ions in the case of the oxidized peptide. In Fig. 6*B*, the MS spectra of the singly oxidized peptide in the absence of calcium are shown. The y-type series ions y_{2-10} are unchanged upon comparison to the spectrum of the unmodified peptide in *panel A*, whereas ions y_{11-13} are shifted by +16 atomic mass units. For the b-type series, ions b_{5-14} clearly show mass shifts of +16 atomic mass units. No amount of the unmodified form for y_{11-13} and b_{5-14} ions was observed above the noise level. This indicates that phenylalanine 125 on the N-terminal end of the peptide is the only residue oxidized, consistent with the solvent accessibility data for the inactive gelsolin. Fig. 6*C* shows the MS/MS spectrum of the doubly protonated ion for the singly oxidized peptide 121–135 that was oxidized in the presence of 0.5 mM EGTA and 200 μM Ca^{2+}. Clearly, the y_{11} and b_{13} ions are shifted by +16 atomic mass units, while the y_2 and b_{3-4} ions are observed unchanged with respect to the unmodified peptide fragment. This indicates that oxidation can take place on the N-terminal or C-terminal ends of the peptide under these conditions. Further examination of the ion series reveals that y_{11} and b_{13} show no unmodified fragment product, whereas y_{3-10} and b_{5-12} ions show both unmodified and modified products. Thus, it is clear that residues Phe-125 and Tyr-133 are modified during the radiolysis experiment for calcium-activated gelsolin. Moreover, the relative abundances for the y_{3-10} and b_{5-12} fragment ions shifted by +16 atomic mass units are almost equal to that for the unshifted fragments. Because the unmodified and modified peptide ions have similar structures and collision efficiencies and the instrumental parameters such as trapping and detection efficiencies are controlled in this experiment, the intensity of the ion signals in the MS/MS spectrum can be semiquantitatively analyzed. Phe-125 and Tyr-133 residues (under Ca^{2+} conditions) have similar reactivity and appear to be equally accessible to the solvent.

All oxidized peptides (in the absence and presence of Ca^{2+}) were analyzed by tandem mass spectrometry in a similar manner. This analysis defined the oxidized side chains for each peptide as shown in Table I. On binding of 200 μM Ca^{2+}, eight additional residues were detected as exposed within the gelsolin sequence. Their locations in the gelsolin structure are displayed in Fig. 7 (*panels A–C*), including Tyr-68 and Leu-71

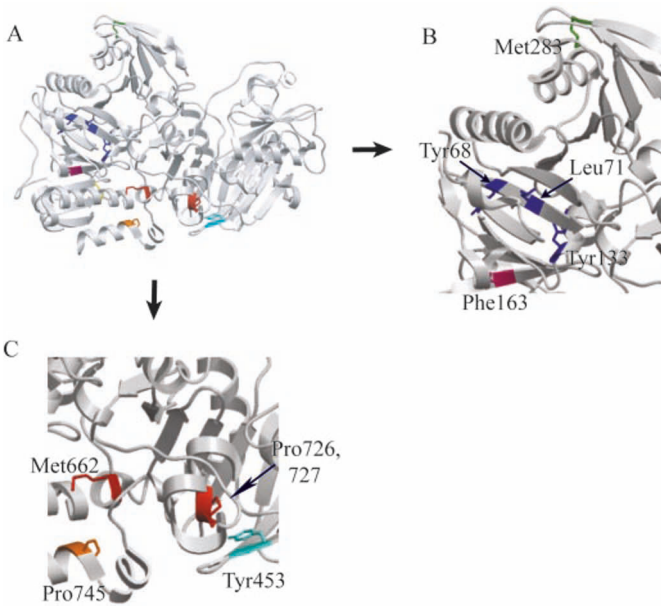

FIG. 7. *A*, representation of the S1–S6 gelsolin structure indicating residues oxidized only in the presence of Ca^{2+} within S1 (*blue*), S2 (*magenta*), S3 (*green*), S4 (*cyan*), S6 (*red*), and the C-terminal tail (*orange*). *B* and *C*, illustration of the buried residues, including Tyr-68 (S1), Leu-71 (S1), Tyr-133 (C terminus of S1), Phe-163 (S2), Tyr-453 (S4), Pro-726 and -727 (S6), and Pro-745 (tail of S6), that are revealed in the presence of Ca^{2+}. Met-283 (S3) and Met-662 (S6) showed decreases in oxidation rate. The color coding used in *panels B* and *C* is as described for *panel A*.

in the β-sheet of S1, Tyr-133 at the C-terminal end of S1, and Phe-163 on an F-actin-binding segment of S2 (*panel B*) as well as Tyr-453 in the β-sheet of S4, Pro-726 and Pro-727 in S6, and Pro-745 in the C-terminal tail (*panel C*). It is important to emphasize that depicted residues are located within peptides that exhibited increases in the oxidation rate upon Ca^{2+} binding. Moreover, the side chains of these residues are partially or entirely buried in the inactive gelsolin structure, and their oxidation indicates specific sites that become more exposed as an integral part of the Ca^{2+} activation process. Two residues, including Met-283 (S3) and Met-662 (S6), that showed dramatic decreases in the extent of oxidation in the presence of Ca^{2+} are also noted in Fig. 7 (*panels B–C*). In addition, Fig. 8 (*panels A–E*) illustrates 31 oxidized sites detected by mass spectrometry that did not show changes in the solvent accessibility in the presence of Ca^{2+}. These are located throughout the structure and clearly define regions that do not change their solvent accessibility in response to Ca^{2+} binding.

Protein Footprinting as a Biophysical Probe of Protein Structure and Dynamics in Solution—Radiolytic protein footprinting coupled to MS has been developed over the last several years and has matured into a viable approach for analyzing protein structure and dynamics. Recent work by other investigators has shown that Fenton reagents can also be used as a source of hydroxyl radicals to analyze protein surface modifications (33), and the results obtained from the

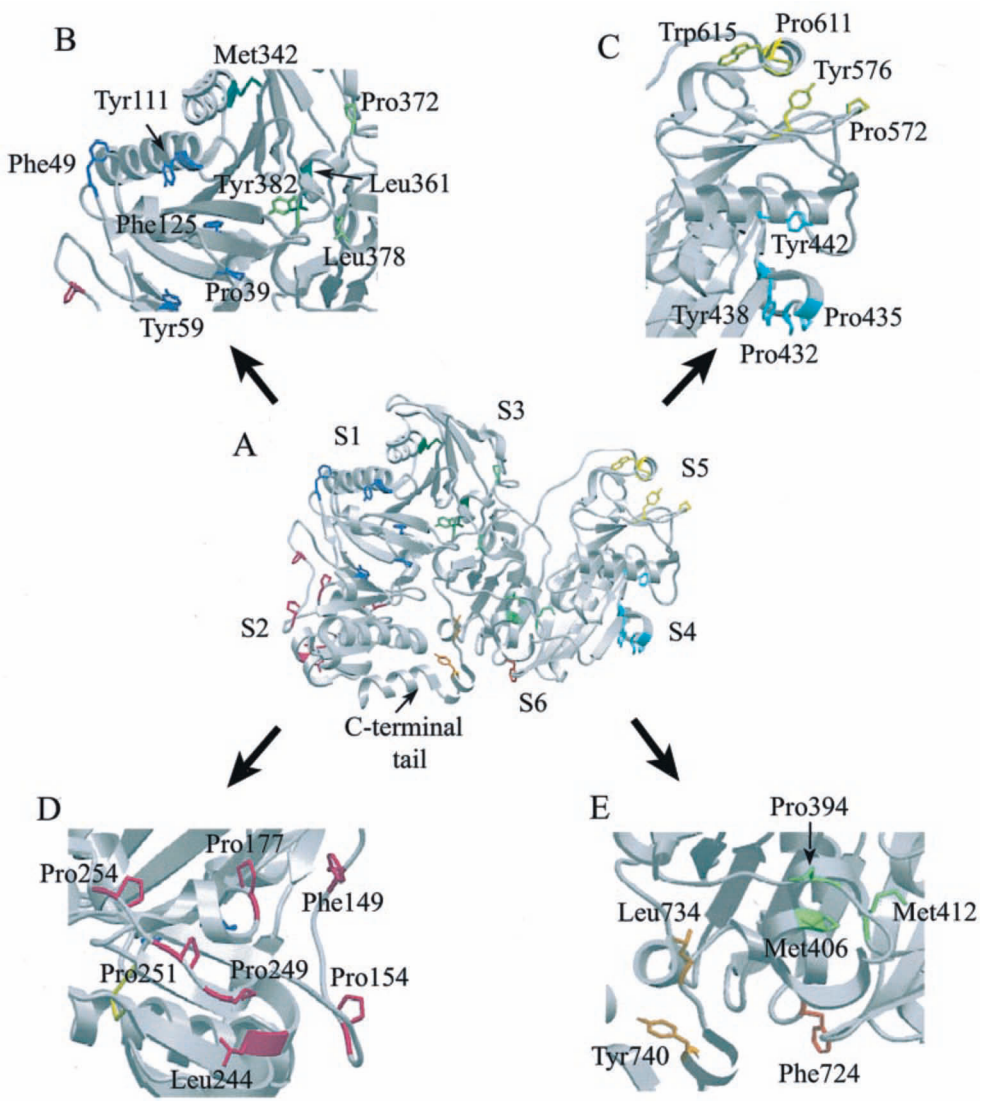

FIG. 8. *A*, subunit structure of gelsolin with residues that show modification in the absence and presence of Ca^{2+} within S1 (*blue*), S2 (*magenta*), S3 (*green*), the S3–S4 subdomain linker (*light green*), S4 (*cyan*), S5 (*yellow*), S6 (*red*), and the C-terminal tail (*orange*). *B*, *C*, *D*, and *E*, illustration of the oxidized residues, including Pro-39, Phe-49, Tyr-59, and Tyr-111 (S1); Phe-125 (S1); Phe-149, Pro-154, Pro-177, and Leu-244 (S2); Pro-249, Pro-251, and Pro-254 (S2–S3); Met-342 (S3); Leu-361 (S3); Pro-372, Leu-378, Tyr-382, Pro-394, Met-406, and Met-412 (S3–S4); Pro-432, Pro-435, Tyr-438, and Tyr-442 (S4); Pro-572, Tyr-576, Pro-611, and Trp-615 (S5); Phe-724, Leu-734, and Tyr-740 (S6), that exhibited oxidation and are Ca^{2+}-insensitive. The residues are color-coded as described for *panel A*.

two methods are comparable (34). Synchrotron radiolysis technique has been successfully applied in the analysis of protein structure (1), protein folding (34), protein-protein interactions (2, 5, 35), protein dynamics (4, 36), and protein-DNA interactions (6). In this paper we provide explicit details of how the method can provide detailed structural information in solution even for a large protein like gelsolin (90 kDa).

In hydroxyl radical-mediated protein footprinting, as for deuterium exchange methods (7–11), the modified protein is subjected to proteolysis. However, in contrast to deuterium exchange, the production of stable modifications through hydroxyl radical exposure allows a wider range of samples as well as protease conditions to be examined under a wide range of solution conditions and pH values and even permits the examination of very large macromolecules. The stable modification of side chains allows a specific probe site to be identified using tandem MS methods, whereas for deuterium exchange, typically the conformational change can only be localized to a specific peptide fragment. The potential disadvantage of x-ray radiolysis is that if a reactive side chain is not present in a particular peptide segment, there are no probes. Thus, extension of the method to include additional side chain probes would be valuable, and is ongoing (37). However, the examination of side chains is complementary to deuterium exchange methods that examine backbone structure.

It must be emphasized that footprinting provides only "lo-

cal" information about the reactivity of the side chain probes. Allosteric changes in conformation induced by ligand binding can also give rise to either protections (decreases in side chain reactivity) or enhancements (increases in reactivity) depending on the induced conformational changes. This must be carefully considered when interpreting data from these experiments, and examples of each of these are provided in this study. This caution is especially pertinent in the examination of protein- or protein-nucleic acid interactions, where the formation of a binding interface gives rise to protections; however, confirmation of the interface should include additional biochemical, structural, or genetic data.

Nuclear magnetic resonance (NMR) spectroscopy is the method of choice for solution structure determination but requires milligram sample quantities of singly or doubly isotopically labeled material, although enhanced sensitivity through cryoprobes and other approaches is improving the situation significantly (38, 39). NMR is difficult to apply to large macromolecules (although advances using TROSY are allowing proteins in the 100-kDa range to be successfully analyzed (40)) and is a challenge for kinetic structural analysis (11, 38, 41). However, inventive NMR approaches, such as deuterium exchange quench studies of protein folding (42, 43), have yielded major insights into conformational dynamics of macromolecules with high structural resolution. Of course the major drawbacks, even for these powerful exchange methods, are 1) the limits on size for the proteins or complexes that can be analyzed, 2) the need for quenching methods to "freeze" the exchange, and 3) the typical necessity in NMR experiments for tens of micromolar to millimolar concentrations of the macromolecules (11, 41). MS methods can be carried out with very small amounts of material; picomoles were used in the present study, but femtomole quantities are clearly feasible with the most modern instruments. Also, footprinting methods are not intrinsically size-limited, as long as the relevant peptides can be detected.

Footprinting has also been successfully applied to examine time-resolved structural changes in nucleic acids during folding (44) and protein binding (45) on the millisecond time scale (27, 46). As seen in this paper synchrotron exposures of proteins for tens of milliseconds provide sufficient oxidation that modified products can be easily detected. Thus, a valuable future application of protein footprinting would be in time-resolved studies. In the context of the investigations seen here, it would be of great interest to observe the time evolution of the calcium-dependent conformational changes seen for gelsolin. The rapid mixing of gelsolin with buffer containing Ca^{2+} and then the exposure of the combined solution to a millisecond dose of radiation could be used to identify structural intermediates in the activation process.

Lastly, one should consider the potential impact of footprinting data on protein structure modeling. Computational methods to analyze and predict protein structure using both energy-derived algorithms as well as those primarily driven by homology considerations have been shown to be quite powerful (47–50). For example, incorporation of solvation effects, including a buried surface area potential in the scoring, has improved the correlation between predicted and measured stabilities of designed proteins (48). Footprinting methods could provide "restraints" on the potential burial or exposure of reactive residues that could be explicitly incorporated into such modeling algorithms, improving the accuracy of such predictions and allowing the modeling of quite distantly related homologs (50, 51).

In conclusion, synchrotron x-ray footprinting is quite valuable as a biophysical technique. It allows examination of temporal changes on time scales of milliseconds with high structural resolution, up to single side chain resolution in the case of proteins. Multiple sites can be independently examined in a single experiment. The amount of sample required to perform an experiment is on the subpicomole levels, and native material can be used. A wide range of solution conditions can be used for footprinting, including the use of urea as a denaturant, without interfering with the radiolysis. Finally, proteins and their complexes can all be examined without intrinsic size limitations.

Acknowledgments—The National Synchrotron Light Source at Brookhaven National Laboratory was supported by the Division of Materials Sciences of the Department of Energy.

* This work was supported by the Biomedical Technology Centers Program, of the National Institute for Biomedical Imaging and Bioengineering P41-EB-01979; by the Innovative Molecular Analysis Technologies Program, NCI, National Institutes of Health Grant R33-CA-84714; and by National Institutes of Health Grant R01-GM-53807. The costs of publication of this article were defrayed in part by the payment of page charges. This article must therefore be hereby marked "*advertisement*" in accordance with 18 U.S.C. Section 1734 solely to indicate this fact.

** To whom correspondence should be addressed: Dept. of Physiology and Biophysics, Albert Einstein College of Medicine, 1300 Morris Park Ave., Bronx, NY 10461-1602. Tel.: 718-430-4136; Fax: 718-430-8587; E-mail: mrc@aecom.yu.edu.

REFERENCES

1. Kiselar, J. G., Maleknia, S. M., Sullivan, M., Downard, K. M., and Chance, M. R. (2002) Hydroxyl radical probe of protein surfaces using synchrotron X-ray radiolysis and mass spectrometry. *Int. J. Radiat. Biol.* **78,** 101–114
2. Guan, J. Q., Vorobiev, S., Almo, S. C., and Chance, M. R. (2002) Mapping the G-actin binding surface of cofilin using synchrotron protein footprinting. *Biochemistry* **41,** 5765–5775
3. Maleknia, S. D., Brenowitz, M., and Chance, M. R. (1999) Millisecond radiolytic modification of peptides by synchrotron X-rays identified by mass spectrometry. *Anal. Chem.* **71,** 3965–3973
4. Kiselar, J. G., Janmey, P. A., Almo, S. C., and Chance, M. R. (2003) Visualizing the Ca2+-dependent activation of gelsolin by using synchrotron footprinting. *Proc. Natl. Acad. Sci. U. S. A.* **100,** 3942–3947
5. Goldsmith, S. C., Guan, J. Q., Almo, S., and Chance, M. (2001) Synchrotron protein footprinting: a technique to investigate protein-protein interactions. *J. Biomol. Struct. Dyn.* **19,** 405–418
6. Rashidzadeh, H., Khrapunov, S., Chance, M. R., and Brenowitz, M. (2003) Solution structure and interdomain interactions of the Saccharomyces cerevisiae "TATA binding protein" (TBP) probed by radiolytic protein footprinting. *Biochemistry* **42,** 3655–3665
7. Katta, V., and Chait, B. T. (1993) Hydrogen/deuterium exchange electros-

pray ionization mass spectrometry: a method for probing protein conformational changes in solution. *J. Am. Chem. Soc.* **115,** 6317–6321
8. Zhang, Z., and Smith, D. L. (1993) Determination of amide hydrogen exchange by mass spectrometry: a new tool for protein structure elucidation. *Protein Sci.* **2,** 522–531
9. Zhang, Z., and Smith, D. L. (1996) Thermal-induced unfolding domains in aldolase identified by amide hydrogen exchange and mass spectrometry. *Protein Sci.* **5,** 1282–1289
10. Zhang, Z., Post, C. B., and Smith, D. L. (1996) Amide hydrogen exchange determined by mass spectrometry: application to rabbit muscle aldolase. *Biochemistry* **35,** 779–791
11. Hoofnagle, A. N., Resing, K. A., and Ahn, N. G. (2003) Protein analysis by hydrogen exchange mass spectrometry. *Annu. Rev. Biophys. Biomol. Struct.* **32,** 1–25
12. Guan, J. Q., and Chance, M. R. (2003) Footprinting methods to examine the structure and dynamics of proteins, in *Encyclopedia of Molecular Cell Biology and Molecular Medicine* (R. Meyers, ed) 2nd Ed., Wiley-VCH Inc., Weinheim, Germany, in press
13. Takamoto, K., and Chance, M. R. (2003) Footprinting methods to examine the structure and dynamics of nucleic acids, in *Encyclopedia of Molecular Cell Biology and Molecular Medicine* (R. Meyers, ed) 2nd Ed., Wiley-VCH Inc., Weinheim, Germany, in press
14. Yin, H. L., and Stossel, T. P. (1979) Control of cytoplasmic actin gel-sol transformation by gelsolin, a calcium-dependent regulatory protein. *Nature* **281,** 583–586
15. Norberg, R., Thorstensson, R., Utter, G., and Fagraeus, A. (1979) F-Actin-depolymerizing activity of human serum. *Eur. J. Biochem.* **100,** 575–583
16. Janmey, P. A., and Stossel, T. P. (1987) Modulation of gelsolin function by phosphatidylinositol 4, 5-bisphosphate. *Nature* **325,** 362–364
17. Burtnick, L. D., Koepf, E. K., Grimes, J., Jones, E. Y., Stuart, D. I., McLaughlin, P. J., and Robinson, R. C. (1997) The crystal structure of plasma gelsolin: implications for actin severing, capping, and nucleation. *Cell* **90,** 661–670
18. Kwiatkowski, D. J., Stossel, T. P., Orkin, S. H., Mole, J. E., Colten, H. R., and Yin, H. L. (1986) Plasma and cytoplasmic gelsolins are encoded by a single gene and contain a duplicated actin-binding domain. *Nature* **323,** 455–458
19. Yin, H. L. (1987) Gelsolin: calcium- and polyphosphoinositide-regulated actin-modulating protein. *BioEssays* **7,** 176–179
20. Ditsch, A., and Wegner, A. (1995) Two low-affinity Ca(2+)-binding sites of gelsolin that regulate association with actin. *Eur. J. Biochem.* **229,** 512–516
21. Allen, P. G., and Janmey, P. A. (1994) Gelsolin displaces phalloidin from actin filaments. A new fluorescence method shows that both Ca2+ and Mg2+ affect the rate at which gelsolin severs F-actin. *J. Biol. Chem.* **269,** 32916–32923
22. Pope, B. J., Gooch, J. T., and Weeds, A. G. (1997) Probing the effects of calcium on gelsolin. *Biochemistry* **36,** 15848–15855
23. Robinson, R. C., Mejillano, M., Le, V. P., Burtnick, L. D., Yin, H. L., and Choe, S. (1999) Domain movement in gelsolin: a calcium-activated switch. *Science* **286,** 1939–1942
24. Wen, D., Corina, K., Chow, E. P., Miller, S., Janmey, P. A., and Pepinsky, R. B. (1996) The plasma and cytoplasmic forms of human gelsolin differ in disulfide structure. *Biochemistry* **35,** 9700–9709
25. Ruiz Silva, B. E., and Burtnick, L. D. (1990) Characterization of horse plasma gelsolin. *Biochem. Cell Biol.* **68,** 796–800
26. Bers, D. M., Patton, C. W., and Nuccitelli, R. (1994) A practical guide to the preparation of Ca2+ buffers. *Methods Cell Biol.* **40,** 3–29
27. Ralston, C. Y., Sclavi, B., Sullivan, M., Deras, M. L., Woodson, S. A., Chance, M. R., and Brenowitz, M. (2000) Time-resolved synchrotron X-ray footprinting and its application to RNA folding. *Methods Enzymol.* **317,** 353–368
28. Maleknia, S. D., Ralston, C. Y., Brenowitz, M. D., Downard, K. M., and Chance, M. R. (2001) Determination of macromolecular folding and structure by synchrotron x-ray radiolysis techniques. *Anal. Biochem.* **289,** 103–115
29. Davies, M. J., and Dean, R. T. (1997) *Radical-mediated Protein Oxidation: From Chemistry to Medicine*, Oxford University Press, Oxford
30. Davies, K. J. (1987) Protein damage and degradation by oxygen radicals. I. General aspects. *J. Biol. Chem.* **262,** 9895–9901
31. Roepstorff, P., and Fohlman, J. (1984) Proposal for a common nomenclature for sequence ions in mass spectra of peptides. *Biomed. Mass Spectrom.* **11,** 601
32. Biemann, K. (1988) Contributions of mass spectrometry to peptide and protein structure. *Biomed. Environ. Mass Spectrom.* **16,** 99–111
33. Sharp, J. S., Becker, J. M., and Hettich, R. L. (2003) Protein surface mapping by chemical oxidation: structural analysis by mass spectrometry. *Anal. Biochem.* **313,** 216–225
34. Chance, M. R. (2001) Unfolding of apomyoglobin examined by synchrotron footprinting. *Biochem. Biophys. Res. Commun.* **287,** 614–621
35. Liu, R., Guan, J. Q., Zak, O., Aisen, P., and Chance, M. R. (2003) Structural reorganization of transferrin C-lobe and transferrin receptor upon complex formation: C-lobe to the receptor helical domain. *Biochemistry*, in press
36. Guan, J. G., Almo, S. C., Reisler, E., and Chance, M. R. (2003) Structural reorganization of proteins revealed by radiolysis and mass spectrometry: G-actin solution structure is divalent cation dependent. *Biochemistry*, in press
37. Xu, G., Takamoto, K., and Chance, M. R. (2003) Radiolytic modification of basic amino acids: New probes for protein footprinting. *Anal. Chem.*, in press
38. Palmer, A. G., Kroenke, C. D., III, and Loria, J. P. (2001) Nuclear magnetic resonance methods for quantifying microsecond-to-millisecond motions in biological macromolecules. *Methods Enzymol.* **339,** 204–238
39. Jonas, J. (2002) High-resolution nuclear magnetic resonance studies of proteins. *Biochim. Biophys. Acta* **1595,** 145–159
40. Pervushin, K. (2000) Impact of transverse relaxation optimized spectroscopy (TROSY) on NMR as a technique in structural biology. *Q. Rev. Biophys.* **33,** 161–197
41. Chance, M. R., Sclavi, B., Woodson, S. A., and Brenowitz, M. (1997) Examining the conformational dynamics of macromolecules with time-resolved synchrotron X-ray 'footprinting.' *Structure* **5,** 865–869
42. Chamberlain, A. K., and Marqusee, S. (1998) Molten globule unfolding monitored by hydrogen exchange in urea. *Biochemistry* **37,** 1736–1742
43. Bai, Y., Sosnick, T. R., Mayne, L., and Englander, S. W. (1995) Protein folding intermediates: native-state hydrogen exchange. *Science* **269,** 192–197
44. Sclavi, B., Sullivan, M., Chance, M. R., Brenowitz, M., and Woodson, S. A. (1998) RNA folding at millisecond intervals by synchrotron hydroxyl radical footprinting. *Science* **279,** 1940–1943
45. Dhavan, G. M., Crothers, D. M., Chance, M. R., and Brenowitz, M. (2002) Concerted binding and bending of DNA by Escherichia coli integration host factor. *J. Mol. Biol.* **315,** 1027–1037
46. Sclavi, B., Woodson, S., Sullivan, M., Chance, M., and Brenowitz, M. (1998) Following the folding of RNA with time-resolved synchrotron X-ray footprinting. *Methods Enzymol.* **295,** 379–402
47. Fiser, A., Feig, M., Brooks, C. L., 3rd, and Sali, A. (2002) Evolution and physics in comparative protein structure modeling. *Acc. Chem. Res.* **35,** 413–421
48. Street, A. G., and Mayo, S. L. (1998) Pairwise calculation of protein solvent-accessible surface areas. *Fold Des.* **3,** 253–258
49. Bolon, D. N., Voigt, C. A., and Mayo, S. L. (2002) De novo design of biocatalysts. *Curr. Opin. Chem. Biol.* **6,** 125–129
50. Eswar, N., John, B., Nirkovic, N., Fiser, A., Ilyin, V. A., Pieper, U., Stuart, A. C., Marti-Renom, M. A., Madhusudhan, M. S., Yerkovich, B., *et al*. (2003) Tools for comparative protein structure modeling and analysis. *Nucleic Acids Res.* **31,** 3375–3380
51. Jaroszewski, L., Li, W., and Godzik, A. (2002) In search for more accurate alignments in the twilight zone. *Protein Sci.* **11,** 1702–1713